JCTC Journal of Chemical Theory and Computation

Article

pubs.acs.org/JCTC

Transfer of Frequency-Dependent Polarizabilities: A Tool To Simulate Absorption and Circular Dichroism Molecular Spectra

Jiří Kessler[†,‡] and Petr Bouř*[,†]

[†]Institute of Organic Chemistry and Biochemistry, Academy of Sciences, Flemingovo náměstí 2, 166 10 Prague, Czech Republic

[‡]Department of Physical and Macromolecular Chemistry, Faculty of Science, Charles University, Hlavova 8, 128 40 Prague, Czech Republic

ABSTRACT: Absorption and circular dichroism spectra reveal important information about molecular geometry and electronic structure. For large molecules, however, spectral shapes cannot be computed directly. In the past, transition dipole coupling (TDC) and related theories were proposed as simplified ways of calculating the spectral responses of large systems. In the present study, an alternative approach better reflecting the chemical structure is explored. It is based on the transfer of complex frequency-dependent polarizabilities (TFDP) of molecular fragments. The electric dipole−electric dipole, electric dipole−electric quadrupole, and electric dipole−magnetic dipole polarizabilities are obtained separately for individual chromophores and then transferred to a larger system composed of them. Time-dependent density functional theory and the sum over states methodology were employed to obtain the polarizability tensors of *N*-methylacetamide, and porphyrin molecules were chosen for a numerical test. The TFDP fails for charge-transfer states and close chromophores; otherwise, the results suggest that this method is capable of reproducing the spectra of large systems of biochemical relevance. At the same time, it is sufficiently flexible to account for a wide range of transition energies and environmental factors instrumental in the modeling of chromophore properties. The TFDP approach also removes the need for diagonalization in TDC, making computations of larger molecular systems more time-efficient.

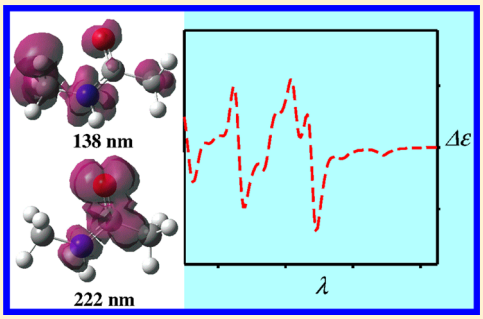

INTRODUCTION

The transfer of spectroscopic properties from fragments to chemically similar residues in a bigger system is an efficient tool for understanding the optical properties of large molecules. For example, the Cartesian coordinates-based transfer (CCT)[1−3] of molecular property tensors[4] and similar approaches[5,6] have made it possible to simulate and interpret vibrational spectra of many large molecules of biological relevance.[2,7−9]

The situation for electronic spectra is quite different. Changes of electronic states are often associated with an extensive rearrangement of the electronic cloud, which can hardly be attributed to individual atoms. Several semiempirical schemes were proposed, such as the coupled oscillator model[10] and the transition matrix theory,[11] where chromophores and their interactions are treated via adjustable parameters. In the simplest transition dipole coupling (TDC) approach, chromophores are replaced by dipoles, and only the electrostatic interaction between them is considered. Encouraging results were obtained, and this was particularly true for biopolymers, including peptides, proteins, and nucleic acids.[12−17] Nevertheless, relatively complicated and mostly ad hoc corrections are necessary to make those approaches more precise and better reflect the chemistry of the system being studied.[18]

For small and medium sized molecular systems, the time-dependent density functional theory (TDDFT)[19] most likely represents the most practical way of obtaining absorption and circular dichroism spectra.[20−23] However, for biopolymers, direct TDDFT applications are limited not only by molecular size but also by the sensitivity of the spectra to environmental and dynamic effects.[24−29] A simplification using rigid Kohn−Sham orbitals has been proposed but has not been found to be sufficiently accurate.[30]

In the present study, we explore the transfer of frequency-dependent polarizabilities (TFDP) as a way of extending accurate ab initio (e.g., TDDFT) approaches to larger systems. The polarizability can be associated with an atom, bond, or a large fragment (chromophore), and it is transferred to a similar unit in the modeled system. Previously, analogous bond polarizability theory[31−33] or the atomic dipole interaction model,[34] breaking molecules down to their components, have already been successfully used to model Raman scattering and vibrational optical activity. The TFDP presented here includes both real and imaginary (dispersion) polarizability components; therefore, it is suitable to provide the electronic spectra as a dispersion part of the total polarizability. Being inherently linked to the chemical structure, the polarizability tensors provide the necessary flexibility to reflect the local chemical environment with the accuracy of TDDFT or other quantum-chemical computations. TFDP is thus better suited to reflect nuances of molecular geometry than previous semiempirical approaches.

Received: February 11, 2015

DOI: 10.1021/acs.jctc.5b00136
J. Chem. Theory Comput. XXXX, XXX, XXX−XXX

This study was also partially inspired by the modern "polarizable embedding" approaches that allow for accurate description of a chromophore entity, whereas longer range interactions are treated in a simpler way.[35,36] These combined quantum-mechanics and molecular-mechanics approaches allow for modeling of a range of effects, including system dynamics, protein or solvent environment, spectroscopic response, and chemical reactivity.[37−39]

We must emphasize, however, that TFDP and other transfer schemes are currently only suitable for weakly interacting (distant) chromophores. For charge transfer and other effects, the transferability concept is not valid, and a rigorous quantum mechanical (at least TDDFT) approach is necessary. Even at the limit of a large separation, the quantum-mechanical and classical (transfer-based) treatment of the chromophores may not converge; however, they are usually close enough to provide a solid basis for prediction and understanding of experimental data.

A solid theoretical basis for interpretation of the absorption and electronic circular dichroism (CD, ECD) spectra is important because of their vast potential in monitoring biomolecular structure and interactions. In particular, ECD (i.e., the differential absorption of the left- and right-circularly polarized visible or ultraviolet light) is very sensitive to molecular structure, conformation, and interactions with the environment.[40−45]

Unlike for previous models,[32,33] the polarizability including the real and dispersive (imaginary) parts is transferred as a function of the frequency. The introduction of a bandwidth parameter (Γ) preventing divergence at the resonant frequencies allows for modeling of light absorption. The theory is formulated in such a way that chromophore polarizabilities can be broken down to atomic ones. We also introduce an arbitrary frequency-dependent dipole polarization density (ρ) useful in the visualization of molecular excitation phenomena and localization of chromophore transitions. Fundamental TFDP properties and comparison with the TDC model are explored for a model *N*-methylacetamide (NMA) dimer. Larger porphyrin and photosynthetic reaction center models are used to document a typical application and as well as limitations of the TFDP approach.

FREQUENCY-DEPENDENT POLARIZABILITIES

Light scattering and absorption on molecules, including chiral phenomena such as differential absorption or scattering of left- and right-circularly polarized light, are conveniently described with the aid of molecular property tensors. The most important ones are the electric dipole−electric dipole (α), electric dipole−magnetic dipole (G'), and electric dipole−electric quadrupole (A) polarizabilities, defined in atomic units as[4,46]

$$\alpha_{\alpha\beta}(\omega) = 2\sum_{j\neq n}\omega_{jn} f_{jn}(\omega)\mathrm{Re}\mu_{nj,\alpha}\mu_{jn,\beta} \tag{1a}$$

$$G'_{\alpha\beta}(\omega) = -2\omega\sum_{j\neq n} f_{jn}(\omega)\mathrm{Im}\,\mu_{nj,\alpha} m_{jn,\beta} \tag{1b}$$

$$A_{\alpha,\beta\gamma}(\omega) = 2\sum_{j\neq n}\omega_{jn} f_{jn}(\omega)\mathrm{Im}\,\mu_{nj,\alpha}\Theta_{jn,\beta\gamma} \tag{1c}$$

$$\alpha^{\nabla}_{\alpha\beta}(\omega) = 2\sum_{j\neq n} f_{jn}(\omega)\mu_{nj,\alpha}\nabla_{jn,\beta} \tag{1d}$$

where the indexes j and n denote excited and ground states, respectively. For exact wave functions, the last expression (1d) is equal to 1a; the gradient form (α^{∇}) of the polarizability is based on dipole-velocity transformation, $\nabla_{jn,\beta} = \omega_{jn}\mu_{jn,\beta}$. In eqs 1a−1d, the sums run over the excited electronic states, n denotes the ground state, $\mu_{nj,\alpha} = \langle n|\mu_\alpha|j\rangle$ corresponds to the electric dipole moment, and an analogous notation is used for the gradient, magnetic dipole $\mathbf{m}$, and electric quadrupole Θ. The Greek indices (α, β, and γ) are reserved for the Cartesian components (x, y, and z), $\omega_{jn} = \omega_j - \omega_n$ is the difference of angular frequencies for each state, and ω is the frequency of illuminating light.

With the transfer in mind, it is important to realize that while α is independent of the choice of coordinate origin, for an origin shift from **O** to **O** + **T**, tensors G' and A change to[4,47]

$$G'_{\alpha\beta} \rightarrow G'_{\alpha\beta} + \frac{1}{2}\omega\varepsilon_{\beta\gamma\delta}T_\gamma\alpha^{\nabla}_{\alpha\delta} \tag{2a}$$

$$A_{\alpha,\beta\gamma} \rightarrow A_{\alpha,\beta\gamma} - \frac{3}{2}(T_\beta\alpha_{\gamma\alpha} + T_\gamma\alpha_{\beta\alpha}) + \sum_{\delta=1}^{3} T_\delta\alpha_{\delta\alpha}\delta_{\beta\gamma} \tag{2b}$$

The frequency function f_{jn} can be written as[4]

$$\begin{aligned} f_{jn}(\omega) &= \frac{\omega_{jn}^2 - \omega^2}{(\omega_{jn}^2 - \omega^2)^2 + \Gamma^2\omega_{jn}^2} \\ &\quad - i\frac{\Gamma\omega_{jn}}{(\omega_{jn}^2 - \omega^2)^2 + \Gamma^2\omega_{jn}^2} \\ &= f_{r,jn}(\omega) + if_{i,jn}(\omega) \end{aligned} \tag{3}$$

where the frequency uncertainty Γ reflects the finite lifetimes of the excited electronic levels in case of resonance ($\omega \approx \omega_{jn}$). For the purposes of spectral modeling, Γ can also be associated with inhomogeneous line broadening. Then, the imaginary ("dispersion") part in eq 3 is responsible for light absorption, and traces of the tensors α and G' directly correspond to the absorption and CD spectra, respectively. For isotropic samples considered in the present study, the contribution of the A tensor to CD intensities vanishes.[4] In particular, when integrating over a selected transition (for $\Gamma \ll \omega_{jn}$), eqs 1a, 1b, and 3 yield

$$\int_{jn}\sum_{\alpha=1}^{3}\alpha_{\alpha\alpha}(\omega)\,\mathrm{d}\omega \cong -i\pi D_{nj} \tag{4a}$$

$$\int_{jn}\sum_{\alpha} G'_{\alpha\alpha}(\omega)\,\mathrm{d}\omega \cong i\pi R_{nj} \tag{4b}$$

where $D_{nj} = \boldsymbol{\mu}_{nj}\cdot\boldsymbol{\mu}_{jn}$ and $R_{nj} = \boldsymbol{\mu}_{nj}\cdot\mathbf{m}_{jn}$ are the usual dipole and rotational strengths, respectively.[48]

We can therefore relate the absorption (ε) and differential ($\Delta\varepsilon$) coefficients, both measured in L mol^{-1} cm^{-1}, to the polarizabilities and angular frequency ω computed in atomic units as follows[48]

$$\varepsilon(\omega) = -\frac{108.7}{\pi}\mathrm{debye}^2\omega^2\sum_{\alpha=1}^{3}\mathrm{Im}\alpha_{\alpha\alpha}(\omega) \tag{5a}$$

$$\Delta\varepsilon(\omega) = 4\times\frac{108.7}{\pi c}\mathrm{debye}^2\omega^2\sum_{\alpha=1}^{3}\mathrm{Im}G'_{\alpha\alpha}(\omega) \tag{5b}$$

where debye = 2.542 and c = 137.5.

DOI: 10.1021/acs.jctc.5b00136
J. Chem. Theory Comput. XXXX, XXX, XXX−XXX

DIPOLE POLARIZATION DENSITY

We introduce the dipole polarization density as an arbitrary tool useful in locating chromophores as spectroscopically active molecular parts. Within a simplified sum over states theory where the excited states were substituted by the TDDFT expansions,[49,50] we calculate the dipole matrix element as

$$\mu_{nj,\alpha} = -\sqrt{2}\sum_{ab} c_{ab}^{j}\int \varphi_a(r) r_\alpha \varphi_b(r)\,\mathrm{d}\mathbf{r} \tag{6}$$

where c_{ab}^{j} are the TDDFT expansion coefficients of state j into single-excited Slater determinants (from an occupied molecular orbital a to a virtual orbital b). By inserting 6 into 1a, we get

$$\alpha_{\alpha\beta}(\omega) = \int \rho_\beta(\mathbf{r},\omega) r_\alpha\,\mathrm{d}\mathbf{r} \tag{7}$$

where we define

$$\rho_\beta(\mathbf{r},\omega) = -2\sqrt{2}\sum_{j\neq n}\omega_{jn} f_{jn}(\omega)\mu_{jn,\beta}\sum_{ab} c_{ab}^{j}\varphi_a(\mathbf{r})\varphi_b(\mathbf{r})$$

as the electric dipole polarization density. The dipole density $\rho_\beta(\mathbf{r},\omega)$ has a real and imaginary part because of the frequency function (eq 3). Most naturally, the absolute value of the density, $\rho = (|\rho_x|^2 + |\rho_y|^2 + |\rho_z|^2)^{1/2}$, can be used as an indication as to which molecular part is the observable transition localized.

DISTRIBUTION OF POLARIZABILITIES OVER MOLECULAR PARTS

In principle, the dipole polarization density defined in the previous section can be used as a tool to refine the distribution of chromophore polarizabilities over individual atoms. However, as the resultant spectra for separated chromophores are rather insensitive to fine distribution changes, this option is not investigated further. Here, we present results where (i) the chromophore is considered to be a point object, and the polarizability is placed to its center of mass, and (ii) the total polarizability calculated for a chromophore is assigned to its atoms with equal weights. The latter option enables estimation of the error associated with the point chromophore approximation.

TRANSITION DIPOLE MODEL

TDC is a well-established method of generating approximate biomolecular spectra[10] and is important as a reference because it is nearly exact for distant chromophores.[51] As detailed implementations may vary, we briefly describe the equations we used. The transition energies (e_i) and electric transition dipole moments ($\boldsymbol{\mu}_i$) obtained by TDDFT for a monomer/chromophore were transferred to each component in a dimer or a larger system. The energies, dipole ($D = \boldsymbol{\mu}_{gk}\cdot\boldsymbol{\mu}_{kg}$) and rotational ($R = \mathrm{Im}\boldsymbol{\mu}_{gk}\cdot\mathbf{m}_{kg}$) strengths for a transition $g \rightarrow k$ in the whole system are obtained via diagonalization of the interaction Hamiltonian.[10,51−54] The diagonal Hamiltonian elements are equal to the transition energies, $H_{ii} = e_i$, and off diagonal elements correspond to the dipole−dipole interaction, $V_{ij} = (r_{ij}^2\boldsymbol{\mu}_i\cdot\boldsymbol{\mu}_j - 3\boldsymbol{\mu}_i\cdot\mathbf{r}_{ij}\boldsymbol{\mu}_j\cdot\mathbf{r}_{ij})/r_{ij}^5$. Then $\boldsymbol{\mu}_{gk} = \sum_j c_j^k\boldsymbol{\mu}_j$ and $\mathbf{m}_{gk} = (i/2)\sum_j c_j^k e_j\mathbf{r}_j \times \boldsymbol{\mu}_j$, where c_j^k are elements of the eigenvectors, and $\mathbf{r}_j$ are electric dipole moment positions. In our computations, we positioned the dipoles in the geometrical center of the HNCO groups (*N*-methylformamide) or in the mass center (porphyrin).

TRANSFER OF FREQUENCY-DEPENDENT POLARIZABILITIES (TFDP)

To obtain spectral properties of a larger system, we calculated the frequency-dependent polarizabilities $\boldsymbol{\alpha}$ and G' defined above for each chromophore by TDDFT and positioned in its mass center. Then, total (complex) polarizabilities of the entire system were obtained as[3,4,55]

$$\alpha_{\alpha\beta} = \sum_i \alpha_{i,\alpha\beta} + \sum_{j\neq i}\Big[\alpha_{i,\alpha\chi}T_{ij,\chi\delta}\alpha_{j\delta\beta} + \frac{1}{3}\big(A_{i\alpha,\chi\gamma}t_{ij,\chi\gamma\delta}\alpha_{j,\delta\beta} - \alpha_{i,\alpha\chi}t_{ij,\chi\delta\gamma}A_{j\beta,\delta\gamma}\big) + \frac{1}{c^2}G'_{i\alpha\chi}T_{ij,\chi\gamma}G'_{j\beta,\gamma}\Big] \tag{8a}$$

$$G'_{\alpha\beta} = \sum_i\Big(G'_{i\alpha,\beta} - \frac{\omega}{2}\varepsilon_{\beta\gamma\delta}r_{i,\gamma}\alpha_{i,\delta\alpha}\Big) - \frac{\omega}{2}\sum_{i\neq j}\Big[\varepsilon_{\beta\gamma\delta}r_{i,\gamma}\alpha_{i,\delta a}T_{ij,ab}\alpha_{j,b\alpha} + \frac{1}{3}\varepsilon_{\beta\varepsilon\delta}r_{i,\varepsilon}\big(\alpha_{j,\alpha a}t_{ij,\lambda\gamma a}A_{i\delta,\lambda\gamma} - \alpha_{i,\delta a}t_{ij,a\lambda\gamma}A_{j\alpha,\lambda\gamma}\big) - \frac{2}{\omega}G'_{i\gamma,\beta}T_{ij,\gamma\delta}\alpha_{j,\delta\alpha}\Big] \tag{8b}$$

where $\mathbf{r}_{ij} = \mathbf{r}_i - \mathbf{r}_j$ is the vector linking the centers of chromophores i and j, and the "distance tensors" are defined as $T_{ij,\alpha\beta} = (3r_{ij,\alpha}r_{ij,\beta} - \delta_{\alpha\beta}r_{ij}^2)(4\pi\varepsilon_0 r_{ij}^5)^{-1}$ and $t_{ij,\alpha\beta\gamma} = \nabla_{i\gamma}T_{ij,\alpha\beta}$. For brevity, we omit the frequency dependence in 8a and 8b. Note that the total polarizabilities are not mere sums of the individual components but also contain terms accounting for the mutual chromophore polarization. For G', an additional term is present due to the origin-dependence of this tensor (see eqs 2a and 8b).

Alternatively to this simpler TFDP approach, chromophore polarizabilities were distributed to individual atoms within the chromophore. For the models (porphyrin, NMA), we considered all atoms in the distribution. Then, the summations in 8a and 8b were run over the atomic indices. We refer to this variant as $\mathrm{TFDP_d}$.

Finally, monomer/chromophore polarizabilities were calculated in the presence of atomic partial charges mimicking the rest of the simulated system/dimer. This "embedded" variant is referred to as $\mathrm{TFDP_e}$. Obviously, the method also enables the "$\mathrm{TFDP_{de}}$" combination (i.e., to estimate chromophore polarizabilities in the presence of partial charges and distribute them to chromophore atoms). The TDC and TFDP models are diagrammatically summarized in Figure 1 as applied to an *N*-methylacetamide dimer.

COMPUTATIONAL DETAILS

Model systems included *N*-methylacetamide (NMA), porphyrin dimers, and a porphyrin cluster derived from the photosystem reaction center.

The geometry of one NMA molecule was optimized by energy-minimization using the Gaussian[56] program suite. The B3LYP[57]/6-311++G** approximation level was chosen as a default, as it previously provided reasonably accurate results in similar studies.[58,59] Other methods (CIS,[60] CAM-B3LYP,[61] LC-wPBE,[62] and TDHF[60]) with the same basis set were performed for control calculations as reported below. Electrostatic charges of NMA for the $\mathrm{TFDP_e}$ method were obtained by the Mulliken (MU) population analysis[63] and by the Merz−Singh−Kollman (MS),[64] CHelp (CHelp),[65] and Hu, Lu, and Yang (HLY)[66] electrostatic field fitting schemes at the B3LYP/6-311++G** level. The dimers were formed by rotation of one NMA molecule by 20° about an axis perpendicular to the NMA plane and shifting it by 4.5, 6.5, and 8.5 Å in a direction perpendicular to that plane (see Figure 2). For the dimers,

DOI: 10.1021/acs.jctc.5b00136
J. Chem. Theory Comput. XXXX, XXX, XXX−XXX

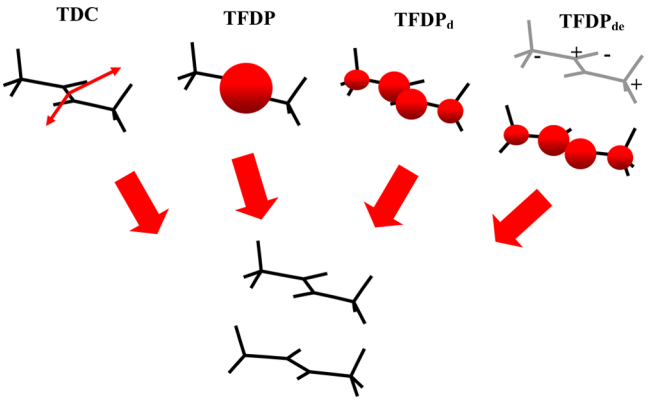

Figure 1. Overview of the transfer scheme used to generate spectra of an NMA dimer. Within the transition dipole coupling model (TDC), transition electric dipole moments (red arrows) are calculated for a monomer and transferred to the dimer components. For the transfer of frequency-dependent polarizabilities (TFDP), the polarizability tensors (symbolized by red circles) are transferred in a similar way. In the TFDP$_d$ variant, the polarizability is distributed over chromophore parts that interact separately after the transfer. By the "e" subscript, we denote a case in which the monomer environment is approximated by atomic partial charges prior to the polarizability computation and transfer.

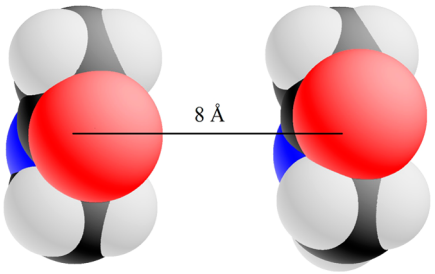

Figure 2. A dimer of two *N*-methylacetamide (NMA) molecules separated by 8 Å; van der Waals atomic radii used for the plot indicate the approximate extension of the electronic cloud. In this case, electron densities of the monomers do not overlap, and it can be expected that the semiempirical transfer schemes provide reasonable results.

absorption and electronic circular dichroism spectra were calculated using the time-dependent density functional theory (TDDFT).[19,20] The frequency-dependent polarizabilities were calculated from the transition moments and excitation energies (i.e., not the Kohn−Sham orbital energies) obtained from the Gaussian output by the SOS approach as outlined elsewhere.[49] Control computation indicated that for a complete set of monoexcited states the SOS method provides virtually the same results as the coupled-perturbed (response) computation but in a shorter time period. The frequency-dependent polarizability components were saved for frequencies covering the entire excitation range incremented in 1 nm steps while applying a frequency uncertainty parameter (Γ) of 10 nm (i.e., variable in the energy-scale) to match the usual experimental band broadening.

We adapted our "cctn" program originally developed for vibrational spectroscopic parameters to enable transfer of the frequency-dependent tensors as well. The transfer is based on the best (least-squares distance method) overlap between the source and target chemical entities and a unitary (rotation) transformation of all Cartesian tensor indices; the details can be found in previous studies.[1−3]

As a "real world" model, we also investigated cyanobacterial photosystem I (Figure 3)[67] for which X-ray coordinates, including 96 porphyrin chromophores, are available as the 1JB0 entry in the protein data bank database (http://www.rcsb.org). A simplified monomer porphyrin molecule (Figure 3) was generated using the 1JB0 coordinates as an initial guess. Minimal relaxation of the geometry was allowed within the constrained (ω_{max} = 300 cm^{-1}, see ref 68) normal mode optimization (NMO)[69,70] at the B3LYP/6-311++G** level and the transition dipole moments and frequency-dependent polarizabilities estimated as for the NMA system. Additionally, two porphyrin dimers were constructed, for which the TFDP and TDC results could be compared to the TDDFT benchmark. The geometries were based on the 1JB0 positions of porphyrins comprising magnesium atom numbers 23357 and 23402, 23.3 Å apart (dimer 1), and magnesia numbers 17407 and 20451, 6.34 Å apart (dimer 2). However, the simplified monomer units lacking the Mg ion were used in the computations. To estimate in detail the computational time, we created larger and smaller arbitrary porphyrin oligomers by adding or deleting other molecules in the 96-mer.

For all systems, eqs 5a and 5b were used to generate the spectra within TFDP using Γ corresponding to the 10 nm

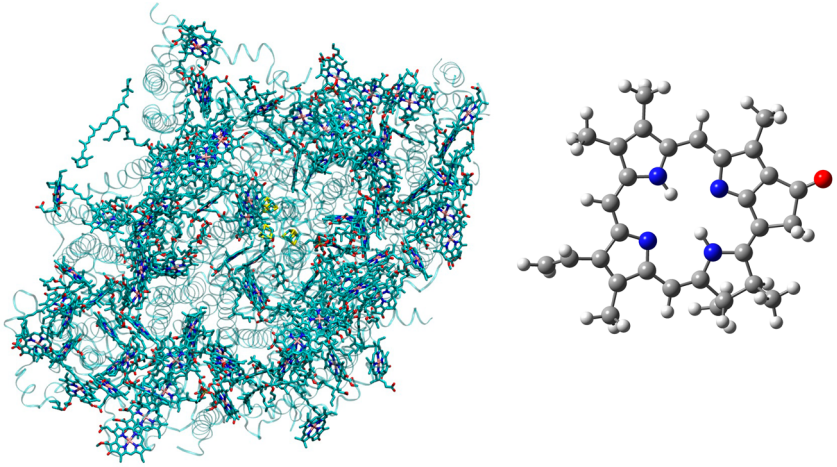

Figure 3. Cyanobacterial photosystem I (from ref 67) with 96 porphyrin residues (left), and a simplified porphyrin monomer (right).

DOI: 10.1021/acs.jctc.5b00136
J. Chem. Theory Comput. XXXX, XXX, XXX−XXX

bandwidth. Likewise, the TDDFT and TDC spectra were generated from the calculated dipole and rotational strengths using Lorentzian bands (full width at half-maximum of 10 nm).

RESULTS AND DISCUSSION

NMA Dipole Polarization Density. In Figure 4, the dipole polarization density (ρ) is plotted as simulated for the NMA molecule at the B3LYP/6-311++G** level for two excitation frequencies corresponding to wavelengths of 138 and 222 nm.

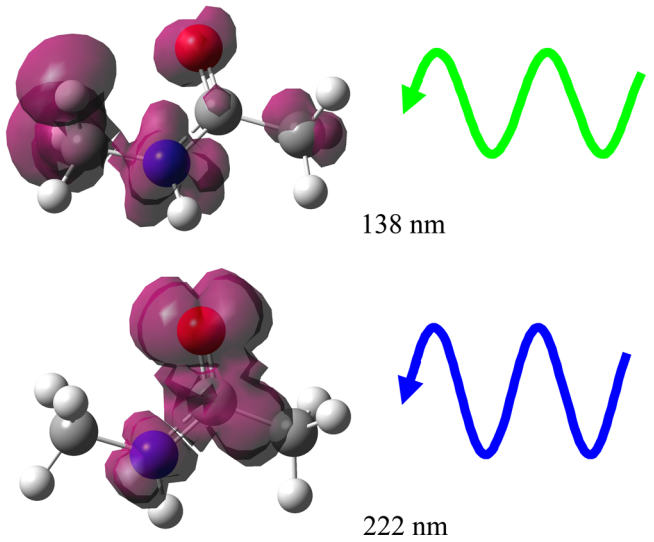

Figure 4. Isodensity surfaces of the dipole polarization density (ρ, see eq 7) for NMA calculated for two excitation wavelengths.

The density corresponds well to the expected properties of the amide chromophore[71] (e.g., predicted theoretically[72] or detected by Raman resonance experiments[73]). For 200 nm, the amide group (HNCO atoms) itself is most spectroscopically active due to the conjugated π-electrons and oxygen electron lone pairs. On the other hand, at 138 nm, it is the aliphatic part of the molecule that is most excited. The dipole polarization density can thus be used as a tool to localize molecular transitions. It justifies the transfer concept based on the locality of some molecular electronic properties and enables us to localize and visualize the relevant electronic transitions.

Distance Dependence of the Dimer Spectra. In Figure 5 (part A), absorption and ECD spectra for three NMA dimers with separation distances of 4.5, 6.5, and 8.5 Å are simulated by TFDP and compared to the benchmark TDDFT computation. As expected, for 4.5 Å in which excited electronic states involving charge-transfer between the NMA molecules significantly contribute to spectral intensities, ECD spectra obtained by the TFDP and TDDFT methods are rather different. Only some spectral features are approximately reproduced, such as the mostly negative signal within 180−200 nm, a positive one within 145−180 nm, and a negative lobe at 135 nm.

Much smaller differences can be found between the TFDP and TDDFT absorption spectra. This reflects the fact that, for separations allowing for a meaningful transfer, the absorption of any chromophore system is always nearly a sum of individual monomers (even for very close separations, the integrated absorption is always proportional to the number of electrons contained in the system;[4] these cases, however, are not investigated here). The main factor determining the splitting of energy levels is the dipole−dipole interaction, where the energy

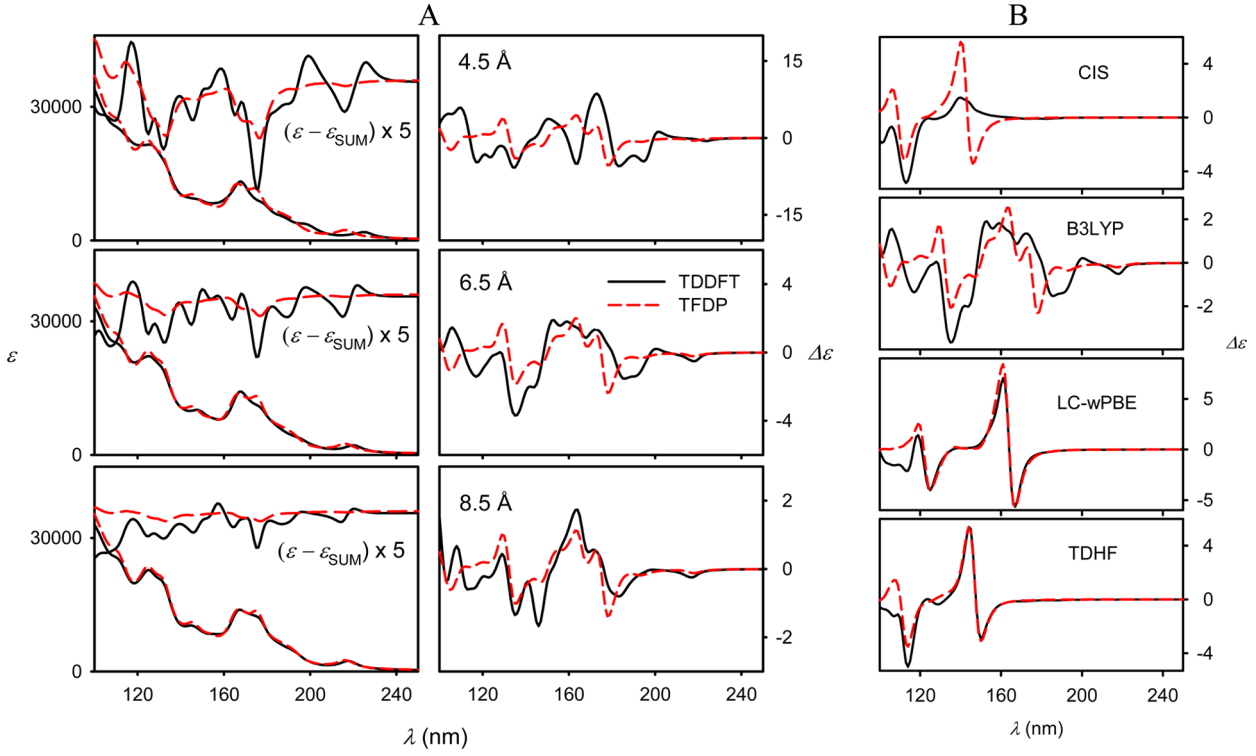

Figure 5. A: Absorption (left) and ECD (right) spectra of an NMA dimer with monomers separated by 4.5, 6.5, and 8.5 Å comparing TDDFT and TFDP. In the absorption panels, the intensity differences with respect to a plain sum of two NMA monomers are plotted as well ($\varepsilon = \varepsilon_{SUM}$, multiplied by 5). B: ECD spectra of the 6.5 Å NMA dimer modeled at the CIS, B3LYP, LC-wPBE, and TDHF levels.

DOI: 10.1021/acs.jctc.5b00136
J. Chem. Theory Comput. XXXX, XXX, XXX−XXX

difference is approximately $\mu_1\mu_2/r^3$, where r is the chromophore distance. For the 215 nm NMA transition, for example, the calculated transition dipole moments were $\mu_1 = \mu_2 = 0.51$ debye, which for the 4.5 Å dimer results in a wavelength splitting of only 0.07 nm. This is further reduced to 0.02 and 0.01 nm for the 6.5 and 8.5 Å dimers, respectively. Note that the mechanism providing the ECD signal is fundamentally different; the monomer ECD is zero, and ECD is thus fundamentally more sensitive to proper modeling of the interchromophore interaction.

For the absorption changes to be emphasized, differences with respect to the sum of the two monomers is inset in the absorption panels. A closer inspection thus reveals small variations, such as very different positions of the longest-wavelength peak (216 nm by TFDP vs 225 nm by TDDFT), and the signal split around 170 nm predicted by TFDP but not by TDDFT. Also, the integral (average) TDDFT absorption intensity in the displayed region is slightly higher than for TFDP by ∼4% in the displayed interval of wavelengths.

At 6.5 Å, the absorption spectra yielded by the two methods are nearly identical. The differences between the TDDFT and TFDP spectra are smaller than for 4.5 Å for both absorption and CD. The TFDP curve mimics several TDDFT CD features reasonably well, such as the positive/negative signal around 130 nm, positive signal within 150−170 nm, and a negative peak at 217 nm. Around 180 nm, although both approaches provide a negative lobe, the exact positions of the minimum differ (179 nm for TFDP vs 186 nm for TDDFT). The TDDFT method additionally predicts a shoulder at 191 nm, which is not reproduced by TFDP. For the 6.5 Å distance, the default B3LYP results are compared to the CIS, LC-wPBE, and TDHF calculations in Figure 5B. The CAM-B3LYP functional provided results very similar to LC-wPBE and are not shown. We can see that for cases in which the charge-transfer states are supposed to be limited[61] (LC-wPBE, TDHF), the TFDP transfer results are closer to those obtained by the reference quantum-mechanical model; on the other hand, the CIS rigid molecular orbital treatment[60] results in rather delocalized states, and the transfer performs less successfully.

For the distance of 8.5 Å, a direct interaction of the NMA electronic clouds (approximately delimited by the van der Waals radii, see Figure 2) is almost excluded, and the influence of intermolecular charge-transfer transitions is limited. The TFDP and TDDFT spectra in Figure 5 are thus even more similar, although minor differences still occur. For example, the negative TFDP CD signal at 146 nm is predicted by TDDFT as a shoulder only. Overall, however, the TFDP seems to be suitable for simulating spectra of distant chromophores.

The transferability or charge-transfer phenomena preventing it can be indicated by the shapes of molecular orbitals involved in the electronic transitions. This is shown in Figure 6, where the lowest-unoccupied molecular orbital (LUMO) in the 6.5 Å dimer largely extends over the intermonomer space, thus facilitating the charge-transfer phenomena. On the other hand, for the separation of 8.5 Å, LUMO is predominantly localized on individual NMA molecules, and a direct quantum-chemical interaction is limited.

Comparison of the Transfer Models. For the 8.5 Å NMA dimer, absorption and ECD spectra simulated with the TDC, TFDP, $TFDP_d$, $TFDP_{de}$, and TDDFT approaches are compared in Figure 7. We can see that the TFDP transfer provides spectral shapes that are very close to the TDC model. Unlike TDC, TFDP also comprises contributions of the

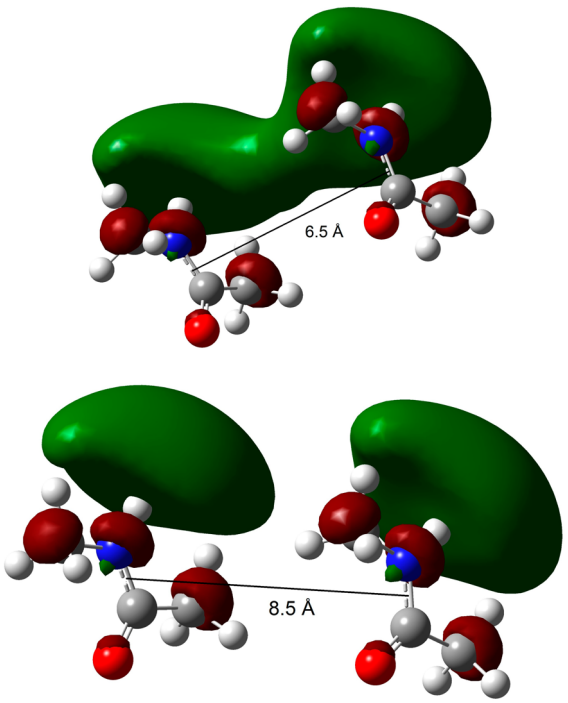

Figure 6. Lowest-unoccupied molecular (LUMO) orbital in the NMA dimer for monomer−monomer separation distances of 6.5 and 8.5 Å.

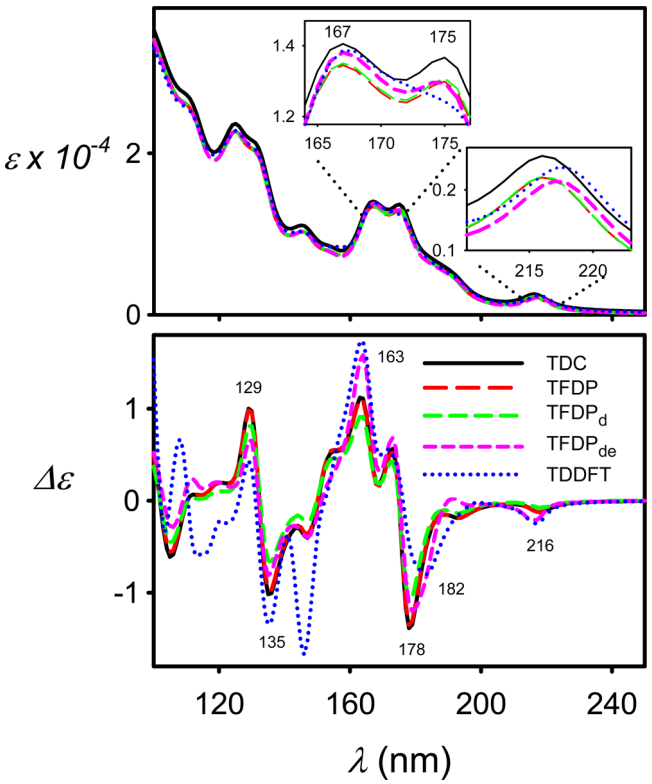

Figure 7. Absorption (top) and ECD (bottom) spectra of the NMA dimer (8.5 Å) as obtained by the TDC, TFDP, $TFDP_d$, $TFDP_e$, and TDDFT approaches; two absorption regions are enhanced in the insets.

quadrupole and magnetic-dipole containing terms (see eq 8); however, their contribution is rather limited for distant chromophores.[3,9] As expected, all approaches provide very

DOI: 10.1021/acs.jctc.5b00136
J. Chem. Theory Comput. XXXX, XXX, XXX−XXX

similar absorption intensities; the TDC approach is only slightly higher than for those obtained by other models.

$TFDP_d$ ECD spectra differ only slightly from those of TFDP; intensities of the peaks at 129, 135, 163, and 178 nm differ by ~15%. The $TFDP_{de}$ variant (accounting for the Mulliken charges mimicking the second chromophore) differs more from TFDP and often favorably approaches the TDDFT standard. A subtle change occurs at the longest-wavelength absorption peak that shifts from 216 nm ($TFDP_d$) to 217 nm ($TFDP_{de}$), which is closer to the TDDFT result (218 nm). Around 216 nm, the negative ECD peak given by $TFDP_{de}$ is nearly identical to that from the TDDFT curve. $TFDP_{de}$ also gives the best match for the negative ECD peak at 182 nm. A spectacular improvement owing to the $TFDP_d \rightarrow TFDP_{de}$ step occurs at 163 nm, where the ECD intensity nearly doubles and closely approaches the TDDFT value. For the shorter-wavelength region (<160 nm) comprising high-energetic delocalized excitations, the transfer approach is apparently not that suitable; however, these transitions are irrelevant for most biospectroscopic applications.[71,74] The 145 nm negative TDDFT ECD band, for example, is a charge-transfer transition from the HOMO−2 π orbital localized on one NMA molecule to a LUMO+17 orbital delocalized (almost Rydberg-type) over the whole dimer. Therefore, none of the transfer approaches can reproduce it.

The effect of charge variations in the $TFDP_e$ model is shown in Figure 8. The absorption and ECD spectra of the NMA dimer (8.5 Å) are plotted as obtained with the Mulliken, CHelp, HLY, and MK charges used for the monomer calculation and compared to the TFDP and TDDFT results. All of the charges appear to give very similar spectral changes. Closer inspection reveals that the effects of the CHelp, HLY, and MK charges are very similar, whereas the Mulliken results are the most distinct. In fact, the MU charges in $TFDP_e$ provide the best agreement with TDDFT, as can be documented by the negative ECD band at 182 nm, the positive signal at 200 nm, and the absorption peak at 218 nm. Admittedly, the variations are rather subtle. Still, this is a somewhat surprising result and may be attributed to an accident as the MU population scheme, unlike the others, was not primarily designed to reproduce the electrostatic field of the NMA molecule.

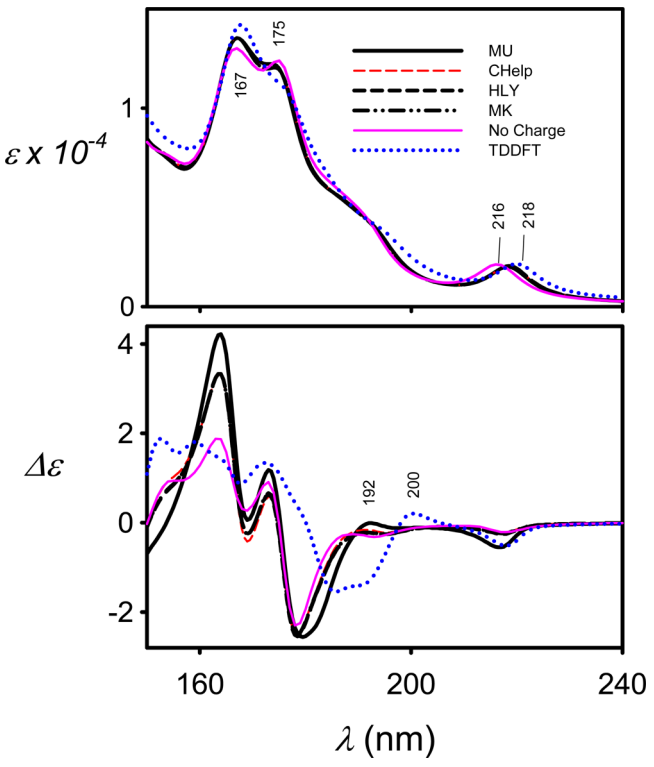

Figure 8. Absorption (top) and ECD (bottom) spectra of the NMA dimer (monomer separation distance of 8.5 Å) as obtained by the $TFDP_e$ model using the MU, CHelp, HLY, and MK charges (as well as no charge) in the transfer as well as the TDDFT result.

Computational times needed to generate the NMA dimer (8.5 Å) electronic spectra are listed in Table 1. The TDC, TFDP, and $TFDP_d$ methods involve computation of electronic excited states for only one molecule. In NMA, molecular symmetry (C_S) can additionally be used for a minor acceleration, reducing the CPU time to 51 min. In $TFDP_e$, the lack of symmetry and the presence of charges almost doubled the computational time to 98 min because each monomer is unique. Still, significant time savings is achieved compared to the full TDDFT calculation lasting 30 h.

Table 1. Computational Times[a] Needed for Various Transfer Models (2000 Dimer Transitions, B3LYP/6-311++G)**

model	time
TDC	51 min
TFDP	51 min
$TFDP_d$	51 min
$TFDP_e$	98 min (2×)
TDDFT	30 h

[a]Intel Xeon CPU E5-2670 0 2.60 GHz.

Note that we chose to test the TFDP method in a wide wavelength interval, and a relatively high number of electronic excited states needed to be calculated to model the whole spectrum. For the NMA dimer, the B3LYP/6-311++G** method provides 396 states within the presented range above 100 nm. Because of the slow decay of the Lorentzian function and the contribution of both real and imaginary polarizability components (ss eqs 3, 8a, and 8b), states below 100 nm slightly contribute to the resultant intensities as well. In practice, however, states below 180 nm are rarely of interest because of the limits of typical spectrometers.

The porphyrin dimer (only CD spectra are plotted in Figure 9) behaves similarly to the NMA dimer. Unlike NMA, however, the inherent chirality of porphyrin (Figure 3) provides a residual CD signal of the monomer ("plain sum" spectra in Figure 9). For a small chromophore separation (6.4 Å, left-hand side), the TDC and TFDP methods are not appropriate. Although they reproduce the increase in intensity, they yield rather unrealistic CD spectral shapes, especially for long-wavelength (~560 nm) transitions. For greater separations (right-hand side), however, both of the approximation methods provide reasonable results. The TFDP CD spectrum is more similar to that of TDDFT, reproducing the fine features around 400 nm and the negative band at 570 nm better.

As indicated in the Introduction, a question arises when TFDP and similar semiclassical methods converge to the exact quantum-mechanical results. Although this topic is very complex and goes beyond the scope of the present study, the results on the NMA and porphyrin dimers suggest two principle limitations of the transfer. First, for close chromophores, the strong nonelectrostatic interaction between

DOI: 10.1021/acs.jctc.5b00136
J. Chem. Theory Comput. XXXX, XXX, XXX−XXX

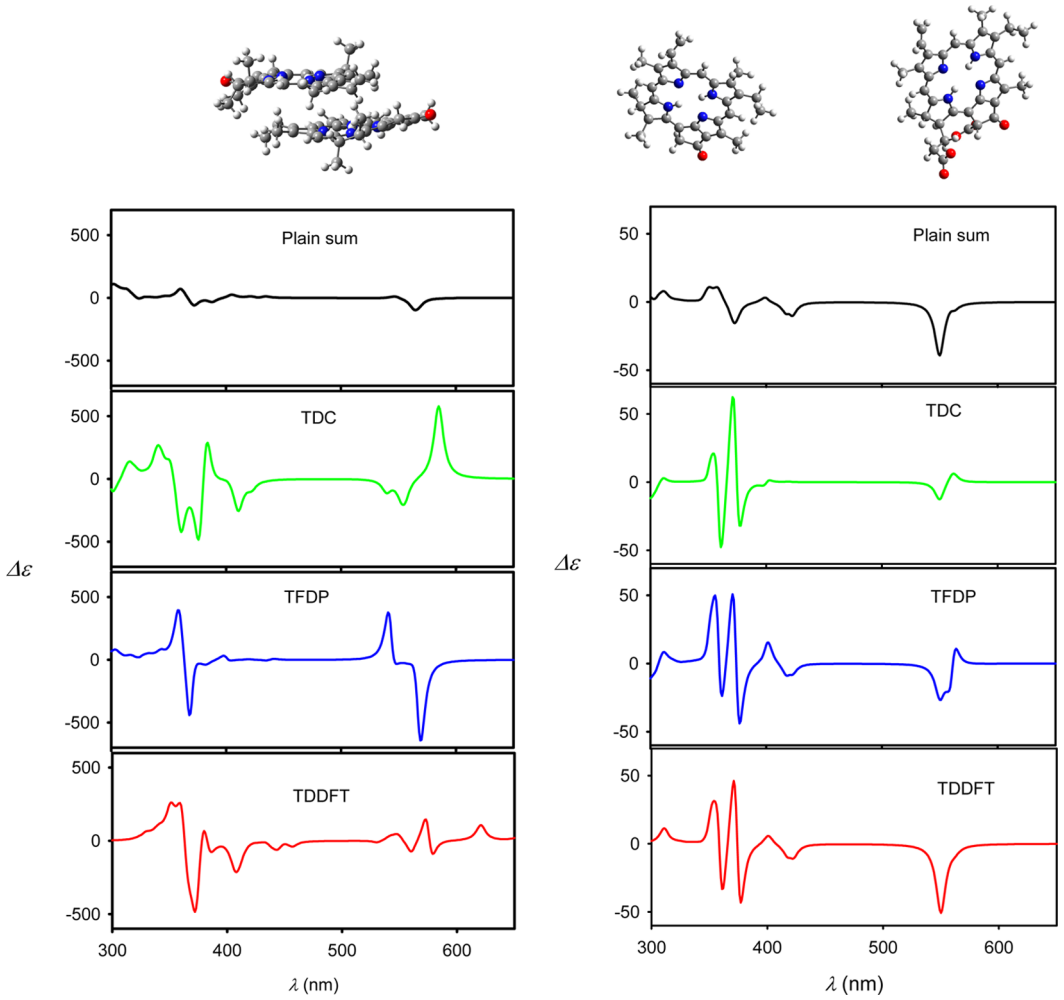

Figure 9. ECD spectra generated for two porphyrin dimers by the four approaches; the distances between the mass centers of the porphyrin monomers were 6.4 Å (left) and 23.3 Å (right).

them cannot be easily described (e.g., using dipole−dipole approximation) and requires the full quantum-mechanical treatment. It is, nevertheless, interesting that even in this case some features in the spectrum can be explained with the empirical models (e.g., the "±" couplet around 360 nm in Figure 9, reproduced by both TFDP and TDDFT). For distant chromophores, the electrostatic interaction between them seems to prevail, which justifies the transfer approach. However, the classical (transfer) and quantum models do not need to converge to the same limit either because of the possibility of charge transfer and delocalized Rydberg-like states. We found it difficult to model the "infinite distance" case because of the limited precision of the quantum-chemical methods optimized for isolated molecules. Fortunately, the classical treatment seems to describe the most important spectral features reasonably well; thus, we find it useful to explore the potential of the transfer methods, such as TFDP. They are computationally efficient, make it easier to understand the light-scattering and absorption phenomena, and are amenable to accuracy improvement in the future (e.g., using more advanced chromophore-embedding schemes).

Finally, we compare the TDC and TFDP CD and absorption spectra generated for the photosystem I-derived 96-mer in Figure 10. We provide this as an example of a potential application only; however, it is noteworthy that the theoretical

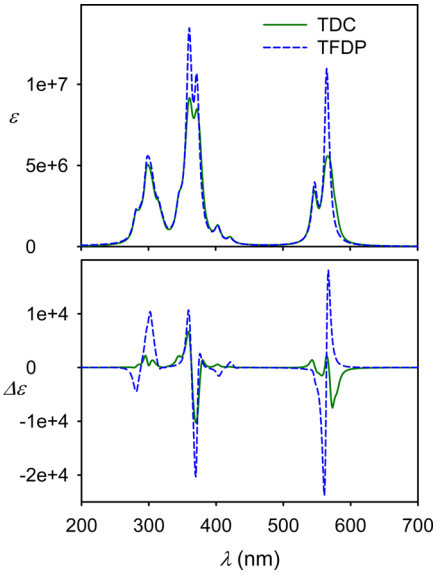

Figure 10. ECD and absorption spectra generated for the porphyrin 96-mer of the photosystem I unit shown in Figure 3

spectra are compatible with an earlier experimental observation in similar systems.[75−77] For illustration, we replot the

DOI: 10.1021/acs.jctc.5b00136
J. Chem. Theory Comput. XXXX, XXX, XXX−XXX

experimental absorption and ECD spinach photosystem spectra from ref 77 in Figure 11. The simplified model used in the present study qualitatively corresponds to the principle experimental features (i.e., the dominance of the Soret; calculated at 380 nm, experimentally around 420 nm), Q (580/680 nm) porphyrin absorption bands,[78] and a relatively large dissymmetry factor (ratio of CD to absorption) within 10^{-2} to 10^{-3}, although a more detailed comparison is not relevant at this stage. The TDC and TFDP models give a similar CD signal in the Soret region (Figure 10), whereas they differ in the Q-bands. The difference can be attributed to many close-distance porphyrin pairs in the photosystem in which case the results from the transfer methods become less predictable, as shown in Figures 5 and 9.

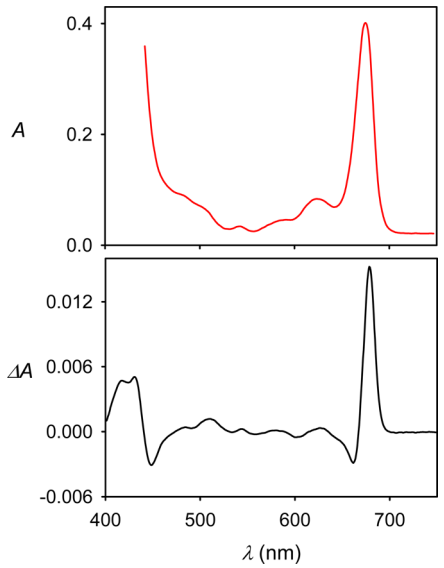

Figure 11. Absorption (A) and ECD (ΔA) experimental spectra of a spinach photosystem according to ref 77. The ECD signal in the Soret region (<400 nm) may be obscured by the large absorption signal.

An interesting insight into the different nature of the TFDP and TDC methods is provided by the dependence of computational time on the system size plotted in Figure 12. Times of TDDFT calculation needed to estimate monomer properties were excluded as they are approximately the same for both methods. From Figure 12 it is obvious that TFDP is not only more time-efficient compared to TDC, but it also has quite different "scaling" with respect to the number of monomer units (N). Indeed, the diagonalization of the interaction Hamiltonian needed for TDC inherently scales as N^3.[79] The computational time also increases sharply due to the many electronic transitions present in the relatively large monomer units. On the other hand, the pairwise interaction described by eqs 8a and 8b for TFDP provides the N^2 scaling, which can further be reduced to almost linear dependence by a preselection of interacting pairs on the basis of interchromophore distances. The state splitting obtained in TDC by the diagonalization is in the TFDP encoded in the shape of the frequency functions.

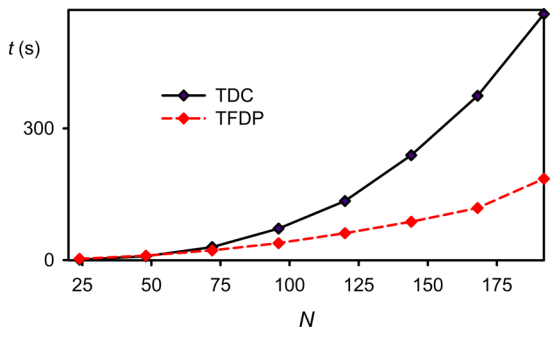

Figure 12. Time required for the TDC and TFDP computation of ECD spectra dependent on the number of porphyrin molecules in an arbitrary oligomer system based on photosystem I.

CONCLUSIONS

In search of transferable quantities that would be widely applicable to simulate optical properties of large molecular systems, we investigated the transfer of frequency-dependent polarizabilities (TFDP). This was significantly facilitated by an efficient TDDFT implementation providing dynamic (frequency-dependent) electric dipole and higher order polarizabilities in a wide range of transition frequencies needed for practical spectroscopy. The TFDP method provided results at least comparable with a similar semiempirical model (TDC). Fine transfer parameters could additionally be varied to account for the chromophore environment and fine polarizability localization, as documented for the $TFDP_d$ and $TFDP_e$ variants. The scaling of TFDP computational time with respect to the system size is also much more favorable than for TDC. Therefore, the polarizability transfer appears to be the method of choice for approximate simulations of electronic spectra for a wide range of large molecular systems.

AUTHOR INFORMATION

Corresponding Author

*E-mail: bour@uochb.cas.cz.

Notes

The authors declare no competing financial interest.

ACKNOWLEDGMENTS

The present study was supported by the Academy of Sciences (M200551205) and Grant Agency (P208/11/0105, 13-03978S, and 15-09072S) of the Czech Republic. We thank Dr. R. Pelc for useful comments on the manuscript. We used computational sources covered by MetaCentrum projects number CZ.1.05/3.2.00/08.0144 and LM2010005.

REFERENCES

(1) Bouř, P.; Sopková, J.; Bednárová, L.; Maloň, P.; Keiderling, T. A. *J. Comput. Chem.* **1997**, *18*, 646−659.
(2) Bieler, N. S.; Haag, M. P.; Jacob, C. R.; Reiher, M. *J. Chem. Theory Comput.* **2011**, *7*, 1867−1881.
(3) Yamamoto, S.; Li, X.; Ruud, K.; Bouř, P. *J. Chem. Theory Comput.* **2012**, *8*, 977−985.
(4) Barron, L. D. *Molecular Light Scattering and Optical Activity*; Cambridge University Press: Cambridge, 2004.
(5) Choi, J. H.; Kim, J. S.; Cho, M. *J. Chem. Phys.* **2005**, *122*, 174903.
(6) Stenner, R. S. *J. Phys. Chem. B* **2012**, *116*, 4141−4153.
(7) Yamamoto, S.; Kaminský, J.; Bouř, P. *Anal. Chem.* **2012**, *84*, 2440−2451.
(8) Andrushchenko, V.; Wieser, H.; Bouř, P. *J. Phys. Chem. B* **2004**, *108*, 3899−3911.
(9) Yamamoto, S.; Bouř, P. *Collect. Czech. Chem. Commun.* **2011**, *76*, 567−583.
(10) Holzwarth, G.; Chabay, I. *J. Chem. Phys.* **1972**, *57*, 1632−1635.
(11) Rabenold, D. A. *J. Chem. Phys.* **1980**, *12*, 5942−5946.

DOI: 10.1021/acs.jctc.5b00136
J. Chem. Theory Comput. XXXX, XXX, XXX−XXX

(12) Hirst, J. D. *J. Chem. Phys.* **1998**, *109*, 782−788.
(13) Gilbert, A. T. B.; Hirst, J. D. *J. Mol. Struct.: THEOCHEM* **2004**, *675*, 53−60.
(14) Besley, N. A.; Oakley, M. T.; Cowan, A. J.; Hirst, J. D. *J. Am. Chem. Soc.* **2004**, *126*, 13502−13511.
(15) Jiang, J.; Abramavisius, D.; Bulheller, B. M.; Hirst, D. M.; Mukamel, S. *J. Phys. Chem. B* **2010**, *114*, 8270−8277.
(16) Woody, R. W. *Monatsh. Chem.* **2005**, *136*, 347−366.
(17) Koslowski, A.; Sreerama, N.; Woody, R. W. Theoretical Approach To Electronic Optical Activity. In *Circular Dichroism Principles and Applications*; Nakanishi, K., Berova, N., Woody, R. W., Eds. Wiley-VCH: New York, 2000; pp 97−132.
(18) Bulheller, B. M.; Miles, A. J.; Wallace, B. A.; Hirst, J. D. *J. Phys. Chem. B* **2008**, *112*, 1866−1874.
(19) Jamorski, C.; Casida, M. E.; Salahub, D. R. *J. Chem. Phys.* **1996**, *104*, 5134−5147.
(20) Furche, F.; Ahlrichs, R. *J. Chem. Phys.* **2002**, *116*, 7433−7447.
(21) Furche, F.; Ahlrichs, R.; Wachsmann, C.; Weber, E.; Sobanski, A.; Vögtle, F.; Grimme, S. *J. Am. Chem. Soc.* **2000**, *122*, 1717−1724.
(22) Bak, K. L.; Hansen, A. E.; Ruud, K.; Helgaker, T.; Olsen, J.; Jørgensen, P. *Theor. Chim. Acta* **1995**, *90*, 441−458.
(23) Autschbach, J.; Ziegler, T.; van Gisbergen, S. J. A.; Baerends, E. J. *J. Chem. Phys.* **2002**, *116*, 6930−6940.
(24) Rogers, D. M.; Hirst, J. D. *Chirality* **2004**, *16*, 234−243.
(25) Hirst, J. D.; Colella, K.; Gilbert, A. T. B. *J. Phys. Chem. B* **2003**, *107*, 11813−11819.
(26) Rogers, D. M.; Besley, N. A.; O'Shea, P.; Hirst, J. D. *J. Phys. Chem. B* **2005**, *109*, 23061−23069.
(27) Kaminský, J.; Kubelka, J.; Bouř, P. *J. Phys. Chem. A* **2011**, *115*, 1724−1742.
(28) Cammi, R.; Corni, S.; Mennucci, B.; Tomasi, J. *J. Chem. Phys.* **2005**, *122*, 104513.
(29) Mennucci, B.; Cappelli, C.; Cammi, R.; Tomasi, J. *Chirality* **2011**, *23*, 717−729.
(30) Bouř, P. *J. Phys. Chem. A* **1999**, *103*, 5099−5104.
(31) Long, D. A. *Proc. R. Soc. London, Ser. A* **1953**, *217*, 203.
(32) Barron, L. D.; Clark, B. P. *J. Raman Spectrosc.* **1982**, *13*, 155−159.
(33) Barron, L. D.; Escribano, J. R.; Torrance, J. F. *Mol. Phys.* **1986**, *57*, 653−660.
(34) Prasad, P. L.; Nafie, L. A. *J. Chem. Phys.* **1979**, *70*, 5582−5588.
(35) Olsen, J. M.; Aidas, K.; Kongsted, J. *J. Chem. Theory Comput.* **2010**, *6*, 3721−3734.
(36) List, N. H.; Beerepoot, M. T. P.; Olsen, J. M. H.; Gao, B.; Ruud, K.; Jensen, H. J. A.; Kongsted, J. *J. Chem. Phys.* **2015**, *142*, 034119.
(37) Thellamurege, N. M.; Hirao, H. *J. Phys. Chem. B* **2014**, *118*, 2084−2092.
(38) Droz, M. H.; Zhou, X.; Shedge, S. V.; Wesolowski, T. A. *Theor. Chem. Acc.* **2014**, *133*, 1405.
(39) Nasluzov, V. A.; Ivanova, E. A.; Shor, A. M.; Vayssilov, G. N.; Birkenheuer, U.; Rösch, N. *J. Phys. Chem. B* **2003**, *107*, 2228−2241.
(40) Sreerama, N.; Woody, R. W. Circular dichroism of peptides and proteins. In *Circular Dichroism Principles and Applications*; Nakanishi, K., Berova, N., Woody, R. W., Eds. Wiley-VCH: New York, 2000; pp 601−620.
(41) Keiderling, T. A. Circular Dichroism. In *Circular Dichroism: Principles and Applications*, 2nd ed.; Berova, N., Nakanishi, K., Woody, R. W., Eds. Wiley: New York, 2000; pp 621−666.
(42) Johnson, W. C. CD of Nucleic Acids. In *Circular Dichroism: Principles and Applications*; Berova, N., Nakanishi, K., Woody, R. W., Eds. Wiley-VCH: New York, 2000; pp 703−718.
(43) King, S. M.; Johnson, W. C. *Proteins* **1999**, *35*, 313−320.
(44) Johnson, W. C. *Proteins* **1999**, *35*, 307−312.
(45) McCann, D. M.; Stephens, P. J. *J. Org. Chem.* **2006**, *71*, 6074−6098.
(46) Nafie, L. A.; Freedman, T. B. Vibrational optical activity theory. In *Circular Dichroism. Principles and Applications*; 2nd ed.; Berova, N., Nakanishi, K., Woody, R. W., Eds. Wiley-VCH: New York, 2000; pp 97−131.
(47) Bouř, P. *Chem. Phys. Lett.* **1998**, *288*, 363−370.
(48) Charney, E. *The Molecular Basis of Optical Activity*. Wiley-Interscience: New York, 1979.
(49) Štěpánek, P.; Bouř, P. *J. Comput. Chem.* **2013**, *34*, 1531−1539.
(50) Štěpánek, P.; Bouř, P. *J. Comput. Chem.* **2015**, *36*, 723−730.
(51) Bouř, P.; Keiderling, T. A. *J. Am. Chem. Soc.* **1992**, *114*, 9100−9105.
(52) Tinoco, I. *Radiat. Res.* **1963**, *20*, 133.
(53) Zhong, W.; Gulotta, M.; Goss, D. J.; Diem, M. *Biochemistry* **1990**, *29*, 7485−7491.
(54) Andrushchenko, V.; Bouř, P. *J. Comput. Chem.* **2008**, *29*, 2693−2703.
(55) Janesko, B. G.; Scuseria, G. E. *J. Chem. Phys.* **2006**, *125*, 124704.
(56) Frisch, M. J.; Trucks, G. W.; Schlegel, H. B.; Scuseria, G. E.; Robb, M. A.; Cheeseman, J. R.; Scalmani, G.; Barone, V.; Mennucci, B.; Petersson, G. A.; Nakatsuji, H.; Caricato, M.; Li, X.; Hratchian, H. P.; Izmaylov, A. F.; Bloino, J.; Zheng, G.; Sonnenberg, J. L.; Hada, M.; Ehara, M.; Toyota, K.; Fukuda, R.; Hasegawa, J.; Ishida, M.; Nakajima, T.; Honda, Y.; Kitao, O.; Nakai, H.; Vreven, T.; Montgomery, J. A., Jr.; Peralta, J. E.; Ogliaro, F.; Bearpark, M.; Heyd, J. J.; Brothers, E.; Kudin, K. N.; Staroverov, V. N.; Kobayashi, R.; Normand, J.; Raghavachari, K.; Rendell, A.; Burant, J. C.; Iyengar, S. S.; Tomasi, J.; Cossi, M.; Rega, N.; Millam, J. M.; Klene, M.; Knox, J. E.; Cross, J. B.; Bakken, V.; Adamo, C.; Jaramillo, J.; Gomperts, R.; Stratmann, R. E.; Yazyev, O.; Austin, A. J.; Cammi, R.; Pomelli, C.; Ochterski, J. W.; Martin, R. L.; Morokuma, K.; Zakrzewski, V. G.; Voth, G. A.; Salvador, P.; Dannenberg, J. J.; Dapprich, S.; Daniels, A. D.; Farkas, O.; Foresman, J. B.; Ortiz, J. V.; Cioslowski, J.; Fox, D. J. *Gaussian 09*, revision D01; Gaussian, Inc.: Wallingford, CT, 2009.
(57) Becke, A. D. *J. Chem. Phys.* **1993**, *98*, 5648−5652.
(58) Šebek, J.; Gyurscik, B.; Šebestík, J.; Kejík, Z.; Bernárová, L.; Bouř, P. *J. Phys. Chem. A* **2007**, *111*, 2750−2760.
(59) Šebek, J.; Kejík, Z.; Bouř, P. *J. Phys. Chem. A* **2006**, *110*, 4702−4711.
(60) Foresman, J. B.; Head-Gordon, M.; Pople, J. A.; Frisch, M. J. *J. Phys. Chem.* **1992**, *96*, 135−149.
(61) Yanai, T.; Tew, D.; Handy, N. *Chem. Phys. Lett.* **2004**, *393*, 51−57.
(62) Vydrov, O. A.; Scuseria, G. E.; Perdew, J. P. *J. Chem. Phys.* **2007**, *126*, 154109.
(63) Mulliken, R. S. *J. Chem. Phys.* **1955**, *23*, 2343−2346.
(64) Singh, U. C.; Kollman, P. A. *J. Comput. Chem.* **1984**, *5*, 129−145.
(65) Chirlian, L. E.; Francl, M. M. *J. Comput. Chem.* **1987**, *8*, 894−905.
(66) Hu, H.; Lu, Z.; Yang, W. *J. Chem. Theory Comput.* **2007**, 1004−1013.
(67) Jordan, P.; Fromme, P.; Witt, H. T.; Klukas, O.; Saenger, W.; Krauß, N. *Nature* **2001**, *411*, 909−917.
(68) Hudecová, J.; Hopmann, K. H.; Bouř, P. *J. Phys. Chem. B* **2012**, *116*, 336−342.
(69) Bouř, P.; Keiderling, T. A. *J. Chem. Phys.* **2002**, *117*, 4126−4132.
(70) Bouř, P. *Collect. Czech. Chem. Commun.* **2005**, *70*, 1315−1340.
(71) Berova, N.; Nakanishi, K.; Woody, R. W. *Circular Dichroism Principles and Applications*; Wiley-VCH: New York, 2000.
(72) Goldmann, E.; Asher, S. A.; Mukamel, S. *Phys. Chem. Chem. Phys.* **2001**, *3*, 2893−2903.
(73) Xiong, K.; Punihaole, D.; Asher, S. A. *Biochemistry* **2012**, *51*, 5822−5830.
(74) Johnson, W. C., Jr. Circular dichroism instrumentation. In *Circular Dichroism and the Conformational Analysis of Biomolecules*, Fasman, G. D., Ed. Plenum Press: New York, 1996; pp 635−652.
(75) Harada, J.; Mizoguchi, T.; Tsukatani, Y.; Noguchi, M.; Tamiaki, H. *Sci. Rep.* **2012**, 671.
(76) Shubin, V. V.; Roegner, M.; El-Mohsnawy, E.; Terekhova, I. V.; Schlodder, E.; Karapetyan, N. V. *Appl. Biochem. Microbiol.* **2010**, *46*, 299−307.
(77) Kropacheva, T. N.; Germano, M.; Zucchelli, G.; Jennings, R. C.; Gorkom, H. J. *Biochim. Biophys. Acta* **2005**, *1709*, 119−126.

DOI: 10.1021/acs.jctc.5b00136
J. Chem. Theory Comput. XXXX, XXX, XXX−XXX

(78) Gouterman, M. *J. Mol. Spectrosc.* **1961**, *6*, 138−163.
(79) Press, W. H.; Teukolsky, S. A.; Vetteling, W. T.; Flannery, B. P. *Numerical Recipes in Fortran*, 2nd ed.; Cambridge University Press: New York, 1992.

DOI: 10.1021/acs.jctc.5b00136
J. Chem. Theory Comput. XXXX, XXX, XXX−XXX